Ultrafast Dynamics of o-Nitrophenol: An Experimental and Theoretical Study

ARTICLE *in* THE JOURNAL OF PHYSICAL CHEMISTRY A · AUGUST 2015

Impact Factor: 2.69 · DOI: 10.1021/acs.jpca.5b04900 · Source: PubMed

THE JOURNAL OF PHYSICAL CHEMISTRY A

Article

pubs.acs.org/JPCA

Ultrafast Dynamics of *o*-Nitrophenol: An Experimental and Theoretical Study

Hanna A. Ernst,[†] Thomas J. A. Wolf,[†,‡] Oliver Schalk,[§,∥] Núria González-García,[†] Andrey E. Boguslavskiy,[∥] Albert Stolow,[∥,⊥] Matthias Olzmann,[†] and Andreas-Neil Unterreiner*[,†]

[†]Institut für Physikalische Chemie, Karlsruher Institut für Technologie (KIT), Kaiserstraße 12, 76131 Karlsruhe, Germany

[‡]Stanford PULSE Institute, SLAC National Accelerator Laboratory, Menlo Park, California 94025, United States

[§]AlbaNova University Centre, Stockholm University, Roslagstullsbacken 21, 10691 Stockholm, Sweden

[∥]National Research Council of Canada, 100 Sussex Drive, Ottawa, Ontario K1A 0R6, Canada

[⊥]Departments of Chemistry & Physics, University of Ottawa, 10 Marie Curie, Ottawa, Ontario K1N 6N5 Canada

Supporting Information

ABSTRACT: The photolysis of *o*-nitrophenol (*o*-NP), a typical push−pull molecule, is of current interest in atmospheric chemistry as a possible source of nitrous acid (HONO). To characterize the largely unknown photolysis mechanism, the dynamics of the lowest lying excited singlet state (S_1) of *o*-NP was investigated by means of femtosecond transient absorption spectroscopy in solution, time-resolved photoelectron spectroscopy (TRPES) in the gas phase and quantum chemical calculations. Evidence of the unstable *aci*-nitro isomer is provided both in the liquid and in the gas phase. Our results indicate that the S_1 state displays strong charge transfer character, which triggers excited state proton transfer from the OH to the NO_2 group as evidenced by a temporal shift of 20 fs of the onset of the photoelectron spectrum. The proton transfer itself is found to be coupled to an out-of-plane rotation of the newly formed HONO group, finally leading to a conical intersection between S_1 and the ground state S_0. In solution, return to S_0 within 0.2−0.3 ps was monitored by stimulated emission. As a competitive relaxation channel, ultrafast intersystem crossing to the upper triplet manifold on a subpicosecond time scale occurs both in solution and in the gas phase. Due to the ultrafast singlet dynamics, we conclude that the much discussed HONO split-off is likely to take place in the triplet manifold.

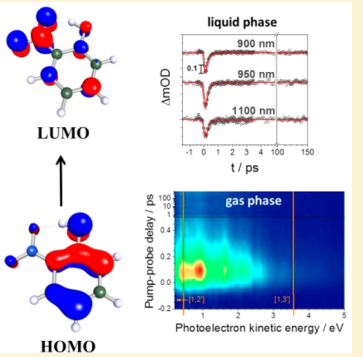

1. INTRODUCTION

The photolysis of *ortho*-substituted nitroaromatic compounds such as *o*-nitrophenol (*o*-NP, Figure 1) is currently discussed as a source of nitrous acid (HONO) in the atmosphere.[1−4] From a structural viewpoint many of these species represent push−pull molecules bearing electron-donating and electron-withdrawing substituents at the aromatic ring.[5] Such push−pull molecules, besides their atmospheric relevance, have attracted continuing general interest due to their unique and manifold intramolecular charge transfer (ICT) properties.[6,7] A prototypical example is the above-mentioned *o*-NP, which exhibits interactions between the nitro and the adjacent hydroxyl group. *o*-NP can serve as a simple model system for ICT dynamics due to the absence of other functional groups and its strong intramolecular hydrogen bond.[8,9] As discussed in previous studies,[10,11] *o*-NP exhibits various ICT transitions upon photoexcitation, but its dynamical relaxation pathways remained unclear. Several photoproducts, e.g., catechol, have been identified in aqueous solution by Boule and co-workers following irradiation in the ultraviolet (UV).[12] These authors found that photoinduced reactions of *o*-NP were much more efficient from electronic states above S_1. Neither fluorescence nor phosphorescence has been reported to date for *o*-NP, which indicates ultrafast radiationless processes. Picosecond time-resolved transient absorption experiments of *o*-NP in benzene, conducted by Takezaki et al.,[13] point to relaxation into the first excited triplet state, T_1, after excitation in the UV. The underlying ISC process, however, remained unresolved due to limited time resolution and could only be estimated to occur on a time scale ≤50 ps.

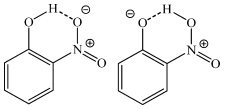

Figure 1. Molecular structure of *o*-nitrophenol (left) and its tautomeric *aci*-nitro form (right).

In atmospheric research, the detection of nitrophenols in the environment has provided impetus for numerous investigations of atmospheric reactions, both in the gas phase and in the condensed phase (clouds, rainwater, fog, and snow).[14−17]

Received: May 22, 2015
Revised: August 10, 2015

DOI: 10.1021/acs.jpca.5b04900
J. Phys. Chem. A XXXX, XXX, XXX−XXX

Nitrophenols are common pollutants[18] and it was noted that *o*-NP, after UV irradiation, could act as a new and previously unappreciated source of nitrous acid.[1] HONO itself was identified as a precursor of hydroxyl radicals which are involved in a multitude of chemical reactions in the atmosphere.[16,17] The mechanism leading to release of HONO after photoexcitation of *o*-NP was proposed to proceed via an intramolecular proton transfer from the hydroxyl to the adjacent nitro group. Theoretical studies of this reaction were based on the assumption that HONO split-off occurs in the first excited triplet state, T_1.[19] A first indication of an intramolecular proton transfer reaction in *o*-NP was provided by detection of the tautomeric *aci*-nitro form (Figure 1) by infrared spectroscopy in low-temperature argon matrices[20] and a resonance Raman investigation.[11] The *aci*-nitro isomer is assumed to be an unstable intermediate in the generation of HONO.[1] Evidence for the *aci*-nitro form by time-resolved experiments, however, has not been reported yet.

Thus, to shed more light on the ultrafast relaxation pathways of *o*-NP in solution and in the gas phase, we applied transient absorption (TA, solution phase) and time-resolved photoelectron spectroscopy (TRPES, gas phase). Our experimental findings were analyzed and rationalized on the basis of results from quantum chemical calculations obtained with density functional theory (DFT) and multireference methods.

2. EXPERIMENTAL AND THEORETICAL METHODS

2.1. Steady State Spectroscopy in Solution and the Gas Phase, Purity of Substances Used. Gas phase and solution spectra were obtained with a UV−vis spectrometer Cary 500 (Varian) in a wavelength range between 200 and 800 nm. The spectra were recorded at room temperature in fused silica cuvettes with an optical path length of 1 mm (solution) and 11.5 cm (gas phase).

o-NP (purity ≥99.5%, Sigma-Aldrich), *n*-hexane (purity ≥98%, Roth), chloroform (purity ≥99.9%, Roth), and 2-propanol (purity ≥99.9%, Roth) were used as purchased. Deionized water was used from our local source.

2.2. Time-Resolved Experimental Methods. *Time-Resolved Photoelectron Spectroscopy in the Gas Phase.* The experimental setup for time-resolved photoelectron spectroscopy of *o*-NP in the gas phase consisted of a femtosecond laser system and a supersonic molecular beam magnetic bottle time-of-flight mass spectrometer, described in detail elsewhere.[21] Briefly, pump pulses with a wavelength of 350 nm were generated as the fourth harmonic of the output of an optical parametric amplifier (TOPAS, Light Conversion), with pulse energies between 1.0 and 2.0 μJ. The probe wavelength was 400 nm at pulse energies between 15 and 20 μJ generated by frequency doubling of the femtosecond laser output. The relative polarization of pump and probe pulses was set to the magic angle. The pulses were collinearly and weakly (f = 50 cm) focused into the interaction region of the magnetic bottle photoelectron spectrometer.

The pump−probe cross correlation was measured by means of nonresonant (1 + 2′) photoionization of nitric oxide to be 110 ± 10 fs. In the approximation of the same length for the pump and probe pulses this value corresponds to 135 ± 10 fs for a (1 + 1′) photoionization using a conversion factor of 1.15. The supersonic molecular beam was generated by a 1 kHz Even-Lavie valve with a 200 μm diameter conical nozzle. The skimmed beam crossed the optical beam path perpendicularly. Helium was used as a carrier gas, with a stagnation pressure of 3.8 bar. *o*-NP was admitted into the body of the valve as a solid. Photoelectron kinetic energies were calibrated by using the well-known photoelectron spectrum of NO.

Time-Resolved Spectroscopy in Solution. The ultrafast dynamics of *o*-NP in solution was studied by femtosecond transient absorption spectroscopy. Pulses of 150 fs duration with 1.6 mJ/pulse at a repetition rate of 1 kHz and a central wavelength of 775 nm were generated by a CPA 2210 laser system (Clark-MXR).[22] The experimental setup is described in more detail elsewhere.[23] The pump wavelength of 350 nm with an energy of 0.7 μJ/pulse was generated by sum frequency mixing.[24] The probe wavelengths between 480 and 1100 nm were generated by a noncollinearly optical parametric amplifier (NOPA) system.[25] Pump and probe beams were focused into the sample using magic-angle polarization geometry. The repetition rate of the laser pulses was reduced by a chopper wheel to allow for measuring the change in the optical density with and without pump-pulse, ΔOD.

The optical density of the samples was set to a value of 3 at the pump wavelength to minimize group velocity dispersion. To avoid the local buildup of photoproducts, the sample solution was flowed continuously through the cuvette, which was made of fused silica with 1 mm optical path length. Data acquisition was performed using in house software in a Labview environment.

2.3. Quantum Chemical Methods. *Single-Reference Methods.* Density functional theory calculations for ground states and time-dependent density functional theory (TD-DFT) calculations for excited states were performed by using the TURBOMOLE V6.3 program package.[26] Geometries of the ground state and the lowest triplet state were optimized with BP86/def2-SV(P).[27−36] Energies at these optimized geometries were computed with B3LYP/aug-cc-pVDZ[27−30,33−39] as well as singlet and triplet excitations and associated oscillator strengths.[40−42]

Multireference Methods. Minimum energy conical intersections (MECIs) between the first excited singlet state and the singlet ground state were optimized using the complete active space self-consistent field (CASSCF) method as implemented in the GAMESS-US (Version R1),[43] with averaging over the two involved states (SA-2-CASSCF).[44] The CAS consisted of seven molecular orbitals (MOs), the four highest occupied and the three lowest unoccupied and eight electrons in combination with the 6-31G(d) basis set. Analysis of the CASSCF wave function showed that the first excited state is well characterized throughout the whole investigated areas of the PES by a single electron LUMO−HOMO transition. Therefore, a smaller CAS involving the highest two occupied and the lowest two unoccupied orbitals and four electrons was employed for further PES scans. In these, a matrix of geometries was produced by changing the distance between the hydrogen atom of the hydroxyl group and the oxygen atom of the closest NO_2 group between 1.8 and 0.8 Å in steps of 0.2 Å as well as the dihedral angle between this oxygen and the phenyl ring plane between 0° and 105° in steps of 15°. For each element of this geometry matrix, the latter two internal degrees of freedom were fixed with all others allowed to relax. At the optimized geometries, energies were calculated with the MCQDPT method.[43,45,46]

3. RESULTS

3.1. Steady State Spectroscopy in Solution and in the Gas Phase. In Figure 2, the measured absorption spectrum of

DOI: 10.1021/acs.jpca.5b04900
J. Phys. Chem. A XXXX, XXX, XXX−XXX

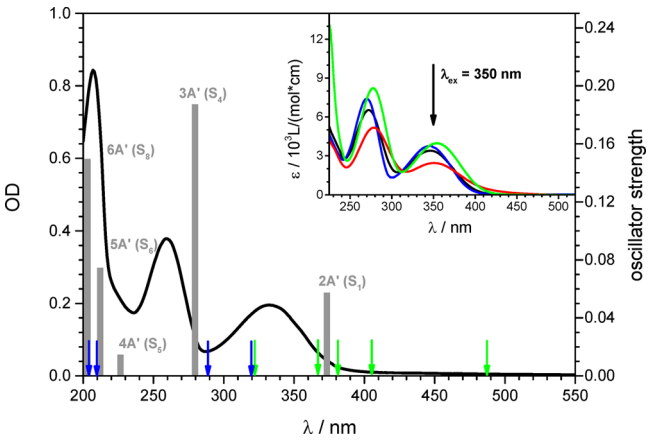

Figure 2. Measured absorption spectrum of gaseous *o*-NP (black line, left axis) and calculated oscillator strengths of selected singlet−singlet transitions to states with A′ symmetry (gray bars, right axis). Singlet−singlet transitions to states with A″ symmetry have by orders of magnitude lower oscillator strengths and are, therefore, marked with blue arrows. Singlet−triplet transitions are marked with green arrows. All computed transitions are related to 1A′ (S_0). Inset graph: absorption spectra measured in solution: *n*-hexane (blue), 2-propanol (black), water (red), and chloroform (green).

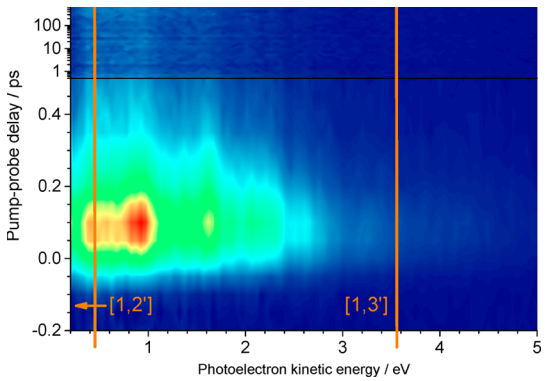

Figure 3. Time-resolved photoelectron spectrum of *o*-NP excited at 350 nm and ionized at 400 nm. The [1,2′] and [1,3′] energetic cut-offs at 0.45 and 3.55 eV, respectively, are indicated by orange lines. For more details see text.

o-NP in the gas phase is shown together with calculated oscillator strengths for selected vertical singlet−singlet transitions with A′ symmetry related to the 1A′ ground state (S_0). Because the oscillator strengths for transitions to states with A″ symmetry are smaller by several orders of magnitude, only the wavelengths of these transitions are marked in Figure 2, along with the wavelengths of singlet−triplet transitions related to 1A′ (S_0). For numerical values, the reader is referred to Table SI1 of the Supporting Information. From Figure 2, it can be seen that gaseous *o*-NP exhibits three absorption bands around 207, 259, and 331 nm, respectively. The positions of these bands are in reasonable agreement with the calculated positions of the vertical transitions (A′ symmetry).

The graph inset in Figure 2 shows the absorption spectra of *o*-NP in different solvents. The first absorption band is centered at 346 nm in both *n*-hexane and 2-propanol, but at 350 nm in water, and 355 nm in chloroform, exhibiting a slight red shift as compared to the gas phase spectrum. These findings are consistent with a previously recorded spectrum in methanol, where the respective absorption band is centered at 349 nm.[10] Because the spectral shifts of the first maxima in the employed solvents are in the range 346−355 nm, the excitation wavelength for all TA experiments in solution was chosen to be 350 nm. According to our assignment above, this corresponds to excitation into the first excited singlet state, 2A′ (S_1). Extinction coefficients of *o*-NP obtained at 350 nm are listed in Table SI2 of the Supporting Information.

3.2. Time-Resolved Photoelectron Spectroscopy in the Gas Phase. The time-resolved photoelectron spectrum of *o*-NP at a pump wavelength of 350 nm (3.54 eV) and a probe wavelength of 400 nm (3.10 eV) is shown in Figure 3. The four lowest ionization potentials (IPs) corresponding to the doublet states D_0 to D_3 of *o*-NP^+ are at 9.29, 10.08, 11.34, and 12.16 eV, respectively.[47] Thus, at time zero at least one pump and two probe photons have to be absorbed ([1,2′], $E_{[1,2']}$ = 9.74 eV) to photoionize *o*-NP. The photoelectron band arising from ionization to D_0 should therefore be found at 0.45 eV kinetic energy. It can also be seen that photoelectron bands lying higher than 0.45 eV are observed: These result from three probe photon ionization ([1,3′], $E_{[1,3']}$ = 12.84 eV). The maximum electron kinetic energy for [1,3′] ionization into the lowest cationic state is, thus, 3.55 eV. Therefore, these photoelectron spectra can be separated into electron kinetic energy regions for [1,2′] and [1,3′] ionization, as shown by the orange lines in Figure 3. Some very weak photoelectron signals beyond the [1,3′] region can be assigned to ionization processes including even more photons. Via [1,3′] ionization the first four cationic electronic states are energetically accessible. Together with additional features most likely due to intermediate Rydberg resonances, this yields the rather complicated photoelectron intensity distribution in the [1,3′] regime seen in Figure 3.

The photoelectron bands appearing at time zero decay rapidly within few hundred femtoseconds, leaving behind a slightly narrower photoelectron band structure stable throughout the investigated time window of 700 ps. Furthermore, the onset of the photoelectron spectrum experiences a slight temporal delay toward lower photoelectron kinetic energies.

Time constants are typically determined from solutions of the convolution integral

$$S(E_{\mathrm{kin}},\Delta t) = \int_{-\infty}^{\Delta t} g(x) \sum_{i=1}^{n} A_i(E_{\mathrm{kin}}) \exp\left(-\frac{\Delta t - x}{\tau_i}\right) \mathrm{d}x \quad (1)$$

with a Levenberg−Marquardt global fitting routine. Here $S(E_{\mathrm{kin}},\Delta t)$ is the time-resolved photoelectron spectrum, which is expressed by the convolution of the experimentally determined Gaussian cross-correlation function $g(\Delta t)$ with a sum of exponential terms containing the decay-associated photoelectron spectrum $A_i(E_{\mathrm{kin}})$ of the process having time constant τ_i. The quantity Δt is defined as $\Delta t = t - t_0$ with t_0 the time zero of the experiment independently determined in cross-correlation experiments.

In the following, we use the indices *gas* and *solv* to distinguish between the time constants derived from experiments in the gas phase and in solution (section 3.3). The TRPES data, shown in Figure 3, is globally fitted with a biexponential decay. Residuals from the 2D fit of TRPES spectrum of *o*-NP are shown in Figure SI1.

The first time constant, $\tau_{1,\mathrm{gas}}$, has a value of 130 ± 10 fs, whereas the value of $\tau_{2,\mathrm{gas}}$ is considerably larger than the investigated range of delay times. A method to account for the

DOI: 10.1021/acs.jpca.5b04900
J. Phys. Chem. A XXXX, XXX, XXX−XXX

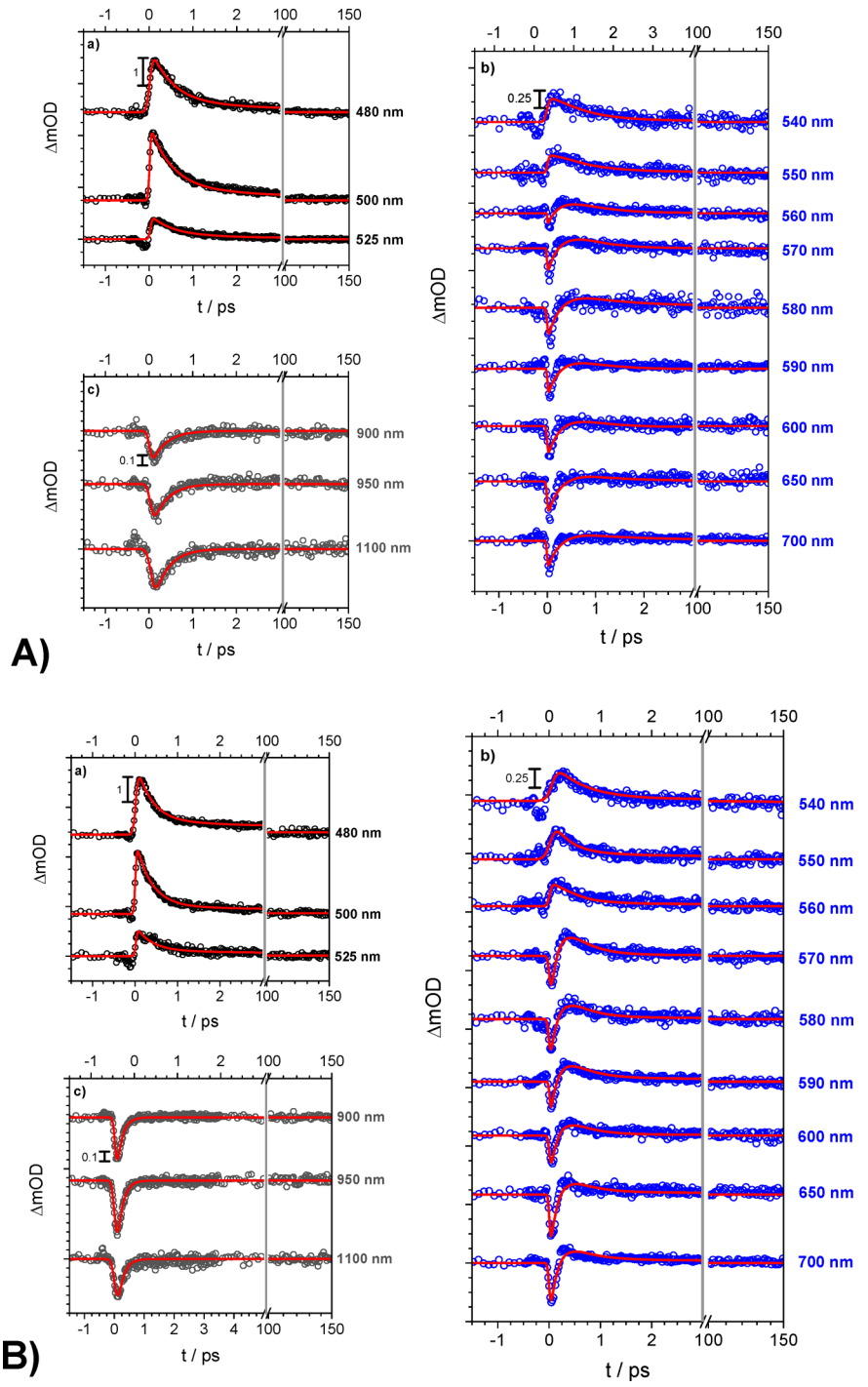

Figure 4. Transient absorption profiles of *o*-NP in water (A) and *n*-hexane (B) at a pump wavelength of 350 nm and probe wavelenghts as labeled. The points represent the absolute experimental values, whereas the red lines are fits. Plots are arbitrarily shifted along the ordinate for better clarity. For explanation of the subpanels (a)−(c), see text.

temporal shift toward smaller photoelectron kinetic energies is the use of $t_0(E_{kin})$ as a fitting parameter. This shift is a sign of large amplitude motion experienced by photoexcited molecule and caused by both the rise of the vertical ionization potential along the large amplitude deformation coordinates and the conversion of potential energy into kinetic energy of the molecule.[48,49] In the present case, treating time zero as an additional fitting parameter yields a shift by 14 ± 6 fs. The decay-associated spectra (DAS) and the visualization of time zero fitting parameters are plotted in the Supporting Information (Figure SI2). A detailed description of using time zero as fit parameter is provided in ref 50 and the corresponding Supporting Information.

3.3. Time-Resolved Spectroscopy in Solution. After excitation into S_1 by a femtosecond pump pulse, the temporal evolution of the population is studied via transient absorption of a time-delayed femtosecond probe pulse. The probe pulse excites molecules into higher states resulting in positive ΔOD values. Conversely, negative ΔOD values can be caused by stimulated emission, as well as ground state bleaching. The

DOI: 10.1021/acs.jpca.5b04900
J. Phys. Chem. A XXXX, XXX, XXX−XXX

latter can be excluded, because our probe wavelengths were in the 480−1100 nm range, which is outside the spectral region where ground state *o*-NP absorbs (Figure 2). Furthermore, ΔOD of the pure solvents was measured to exclude contribution of multiphoton absorption of the solvents and artifacts due to cross phase modulations.

In Figure 4 we show TA profiles of *o*-NP in water and *n*-hexane. The corresponding profiles for chloroform and 2-propanol are displayed in the Supporting Information (Figure SI3), because the transients exhibit only a weak solvent dependence. In general, three different probe wavelength regions can be distinguished. The first, around 500 nm (subpanels a), is characterized by excited state absorption. This feature decays on a subpicosecond time scale, showing a weak residual absorption in *n*-hexane (at 480 nm) and 2-propanol (at 480 and 500 nm) at long delay times within our time window of 500 ps (for a closer inspection of these profiles, see Figure SI4). This residual absorption is too small to be discernible in chloroform and water. In the second region, between 540 and 700 nm (subpanels b), superposition of excited state absorption and stimulated emission is observed. These changes in ΔOD occur over a wide range of probe wavelengths (from 540 to 700 nm) and are almost independent of the solvent. In the third region, between 900 and 1100 nm (subpanels c), only stimulated emission was observed (i.e., no transient absorption).

The TA profiles of *o*-NP were globally fitted with functions analogous to eq 1 with $S(E_{kin},\Delta t)$ substituted by $\Delta OD(\Delta t,\lambda)$ and $A_i(E_{kin})$ substituted by the decay associated difference spectra (DADS) $A_i(\lambda)$.[51] As aforementioned, Δt is defined as difference between t and the experimental time zero t_0. The latter was independently determined in cross correlation experiments of the dye BiBuQ (4,4‴-bis(2-butyloctyloxy)-*p*-quaterphenyl)[52] in 1,4-dioxane at each probe wavelength with the same optical density as the samples. Moreover, the experimental time resolution was obtained from these experiments and found to be always below 200 fs. The quality of the global fits $\Delta OD(\Delta t)$ is demonstrated in Figure 4 as well as in Figure SI3 of the Supporting Information. The time constants obtained for the different solvents are listed in Table 1. For relative amplitudes the reader is referred to the Supporting Information (Tables SI3 and SI4).

Table 1. Time Constants Obtained from Global Fits of the Experimental ΔOD Curves in the Ranges 480−525 nm ($\tau_{1,solv}$, $\tau_{2,solv}$, and $\tau_{3,solv}$) and 900−1100 nm ($\tau_{ind,solv}$), Respectively[a]

	n-hexane	2-propanol	chloroform	water
$\tau_{1,solv}$/ps	0.4 ± 0.1	0.4 ± 0.1	0.5 ± 0.1	0.5 ± 0.1
$\tau_{2,solv}$/ps	9.2 ± 1.2	9.8 ± 1.3	8.0 ± 0.9	3.7 ± 0.3
$\tau_{3,solv}$/ps	>500	>100		
$\tau_{ind,solv}$/ps	0.2 ± 0.1	0.2 ± 0.1	0.3 ± 0.1	0.3 ± 0.1

[a]The error margins represent the statistical errors of the fits.

We found biexponential decays in chloroform and water around 500 nm, described by $\tau_{1,solv}$ and $\tau_{2,solv}$. An additional time constant, $\tau_{3,solv}$, was necessary for *n*-hexane and 2-propanol to model the observed residual transient absorption for long delay times (see Figure SI4 of the Supporting Information for *n*-hexane and 2-propanol). Because $\tau_{3,solv}$ lies outside of our experimental time window of 500 ps only lower bounds can be given. For chloroform and water, the decay associated with $\tau_{3,solv}$ is too weak to be detected. In these cases, residual absorption may be observable for probe wavelengths below the used ones. Furthermore, the stimulated emission in the near-infrared region at 900, 950, and 1100 nm was modeled with a monoexponential decay function using the time constant $\tau_{ind,solv}$. For the intermediate probe wavelengths (540−700 nm), a superposition of transient absorption and stimulated emission occurs. These transients can be sufficiently well described by triexponential decay functions with the time constants $\tau_{1,solv}$, $\tau_{2,solv}$, and $\tau_{ind,solv}$. In this range of wavelengths no long-time absorption was observed and, therefore, $\tau_{3,solv}$ is not significant. We further note that the DADS $A_i(\lambda)$ obtained for the different regimes are difficult to interpret because any analysis of the absolute ΔOD values would require absorption cross sections of electronically excited species, which are not known.

3.4. Quantum Chemical Calculations. *Density Functional Theory.* The optimized geometry of the ground state (S_0) was calculated at the BP86/def2-SV(P) level of theory and shows a planar structure (point group C_s) characterized by a strong intramolecular hydrogen bond (Figure SI5a) of the Supporting Information). From Figure 2, it follows that excitation at 350 nm corresponds to a $S_1 \leftarrow S_0$ transition. As inspection of the molecular orbitals reveals, this excitation is associated with a transition from the highest occupied (HOMO) into the lowest unoccupied molecular orbital (LUMO) characterized by a charge transfer from the hydroxyl to the nitro group. As can be seen from Figure 5, the HOMO is

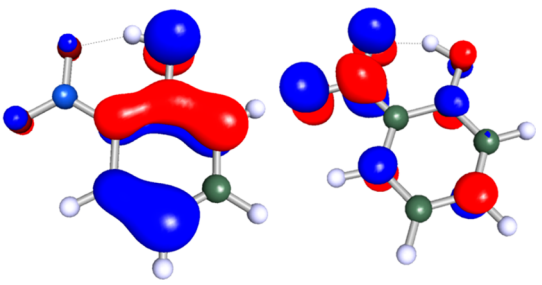

Figure 5. HOMO (left) and LUMO (right) of *o*-NP obtained at the B3LYP/aug-cc-pVDZ level of theory.

described by a π-MO, whereas the main contribution to the LUMO is given by the π^*-MO from the benzene ring and the lone pairs of the nitro group. Thus, the HOMO−LUMO transition can be described as a charge transfer transition into a $^1(\pi\pi^*)$ state.

Because long-lived excited species are observed both in the gas and in the liquid phase, investigation of triplet states becomes important. The optimized geometry of the lowest triplet state T_1 was computed at the BP86/def2-SV(P) level of theory. In analogy to S_0, a planar structure is found, but the hydrogen is transferred from the hydroxyl to the adjacent nitro group (Figure SI5b) of the Supporting Information). Selected triplet excitations relative to T_1 with their corresponding oscillator strengths are calculated and listed in Table 2. It is obvious that the calculations reveal three $T_i \leftarrow T_1$ transitions with significant oscillator strengths namely, at photon energies of 0.79, 2.57, and 3.63 eV.

In view of the promptness of the stimulated emission observed in the TA experiments, the first excited singlet state, S_1, is also of interest. An analogous attempt to optimize the geometry of S_1 at the TD-DFT level failed. These calculations

DOI: 10.1021/acs.jpca.5b04900
J. Phys. Chem. A XXXX, XXX, XXX−XXX

Table 2. Vertical Triplet Excitations Relative to the Optimized Structure of T_1 with Corresponding Oscillator Strengths Calculated at the B3LYP/aug-cc-pVDZ Level of Theory

triplet states	E_{rel}/eV	oscillator strength
T_2	0.79	0.392
T_3	2.57	0.172
T_4	2.68	1.53×10^{-4}
T_5	3.40	1.02×10^{-5}
T_6	3.63	0.825

point toward a transfer of the proton from the hydroxyl to the nitro group and torsion of the formed HONO group out of the ring plane: a stable energy minimum could not be found. The calculations also indicate a close approach of the potential energy surfaces (PES) of S_1 and S_0 during the combined torsion and proton transfer. Because TD-DFT is a ground state method applicable to vertical excitations,[40] its failure in describing excited states that approach the ground state is well-known. Consequently, we performed calculations using multireference methods to get more insights into the excited state properties.

Multireference Methods. A search for a S_1/S_0 minimum-energy conical intersection (MECI) with SA-2-CASSCF confirms the indications from TD-DFT geometry optimizations. The optimized MECI geometry (shown in Figure 6b) mainly differs from the Franck−Condon geometry with respect to two internal degrees of freedom: The hydrogen is transferred to the NO_2 group and the thereby generated HONO group is rotated out of the carbon ring plane by 73°. This angle is defined as 180° minus the dihedral angle (H)CCNO(H). The numerical values of the coordinates are given in the Supporting Information (Table SI5). A quasi three-dimensional plot of the PES for S_0 and S_1 as a function of the two important degrees of freedom, H−O(NO) distance and the HONO torsion angle, is displayed in Figure 6, panel a). The energies were calculated at the positions of the black dots with all other internal coordinates being relaxed. The surfaces shown are two-dimensional spline interpolations.

A more detailed contour plot representation of the relaxed S_1 PES is shown in Figure 6b. It suggests two possible relaxation pathways from the relaxed Franck−Condon geometry to the conical intersection region both with shallow saddle points indicated as SP1 and SP2 in Figure 6b. They mainly differ by the timing between dynamics of the two degrees of freedom. In the pathway over SP1, the hydrogen shift precedes the torsion of the HONO group. In the pathway over SP2 the hydrogen shift follows the torsion. However, conclusions regarding the sequence of intramolecular nuclear motions have to be drawn with caution. Although it is likely that hydrogen atom transfer precedes torsion of HONO due to different reduced masses (excited state intramolecular proton transfers are known to proceed in <50 fs,[53,54] if they are virtually barrierless as in the present case), only detailed trajectory or wave packet calculations could give a decisive answer on actual reaction pathways.

4. DISCUSSION

4.1. Relaxation via Internal Conversion. As mentioned in section 3.4, our CASSCF calculations reveal a close

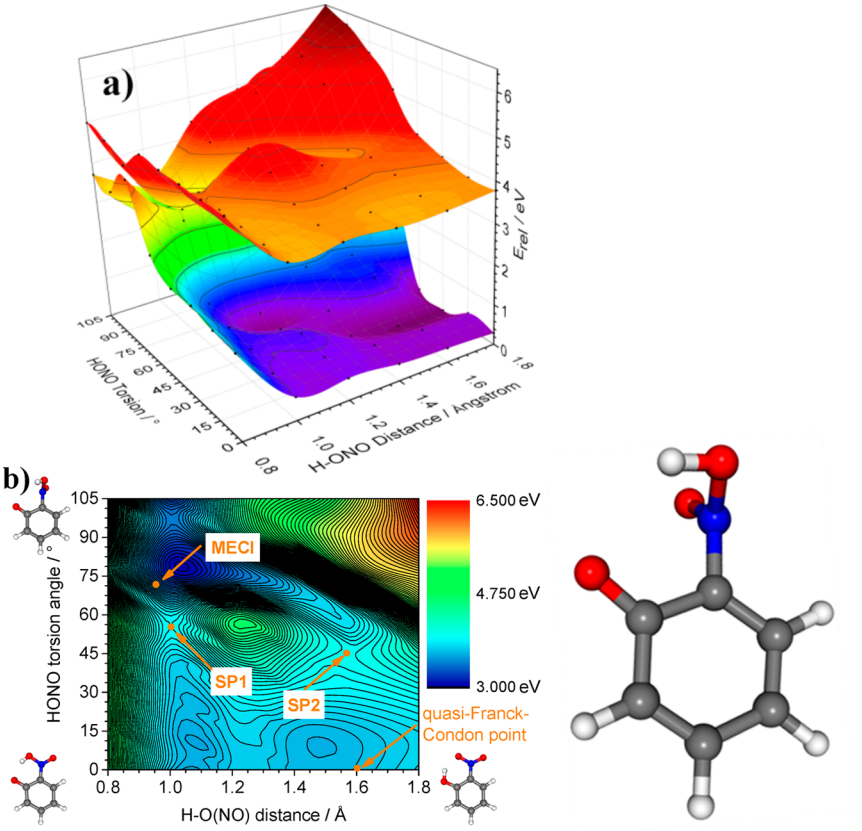

Figure 6. (a) Potential energy surfaces of the S_0 and S_1 state near the Franck−Condon region and the minimum energy conical intersection (MECI). (b) Contour plot of the S_1 PES (left) and structure of *o*-NP at the MECI (right). For details see text.

DOI: 10.1021/acs.jpca.5b04900
J. Phys. Chem. A XXXX, XXX, XXX−XXX

approximation of S_1 and S_0 while decreasing the (O)H−O(NO) distance and subsequently increasing the HONO torsion angle (Figure 6). Hence, the dynamical relaxation from S_1 via a conical intersection to S_0 can be described as a combination of excited state intramolecular proton transfer (ESIPT), triggered by ICT, and HONO torsion. The energy difference between S_1 and S_0 turns out to be more sensitive to the HONO torsional coordinate than to the proton transfer coordinate. From Figures 5 and 6b, it can be concluded that this behavior may be explained by stabilization of the LUMO through a gradual decoupling of donor and acceptor moieties upon increase of the torsion angle.[55,56]

Experimental indication for such changes of the molecular configuration is provided by the observed shift of the onset of the TRPES signal (Figure 3) associated with large amplitude motions in S_1. Taking into account previous studies, typical time constants for intramolecular proton transfer lie on a 10 fs time scale.[53,57] Thus, the observed fast shift in the onset of the photoelectron spectrum of 14 ± 6 fs (section 3.2) in the gas phase can be attributed to proton migration to the *aci*-nitro form of *o*-NP. Because the proton transfer is accompanied by rotation around the C−N bond, as mentioned above, "full" out-of-plane twist of the newly formed HONO group by ∼73° and return to the ground state is supposed to occur on a longer time scale. Consequently, we associate this process with $\tau_{1,gas}$ = 130 ± 10 fs. This time scale suggests a barrierless access to the conical intersection region, a fact that seems to contradict the observation of saddle points on the calculated S_1 PES (Figure 6). However, because the dynamics do not start out on a relaxed PES, the barriers may just not be encountered by the nuclear wave packet.

Taking into account the experimental findings in solution, the most surprising feature of the excited electronic state properties of *o*-NP is the rapid appearance of stimulated emission from the visible to the NIR on a subpicosecond time scale (0.2−0.3 ps) after ICT transition into S_1 in the ultraviolet. Consequently, this behavior points to an expeditious drop of the energy gap between S_1 and S_0 very likely caused by structural changes as predicted by the CASSCF calculations. The observation of the SE itself can be reckoned as an experimental indication for the predicted structural changes in S_1. Thus, the monoexponential decay of stimulated emission between 900 and 1100 nm associated with $\tau_{ind,solv}$ is assigned to depopulation of S_1.

Considering Table 1, the results for $\tau_{ind,solv}$ are quite similar in different solvents. However, as they are close to the time resolution of our experiments, the corresponding decay could also be faster than these values may suggest. Because the energy gap between S_1 and S_0 changes along the relaxation pathway, one might expect a red shift of stimulated emission due to wave packet motion as, e.g., discussed in ref 58. Even though the experimental time zero was independently determined by cross correlation experiments as described in section 3.3, analyses of our data merely reveal an indication in this direction. A clear dependence of the stimulated emission on the employed probe wavelengths, however, is not provided as shown in detail in Figure SI6. Therefore, the ambiguity of the spectral shift is at least in part related to the intrinsic superimposition of the stimulated emission by excited state absorption, which was detected over a wide spectral area. Another reason may be that the wave packet is broadening toward the CI with S_0. For a closer look of the reference experiments as well as of a comparison of selected TA profiles showing stimulated emission at different probe wavelengths the reader is referred to Figures SI6 and SI7, respectively. We also note at this point that $\tau_{ind,solv}$ is not necessarily identical to a time constant describing depopulation of S_1 via a conical intersection with the ground state. The quantity $\tau_{ind,solv}$ can only be considered as a lower boundary for the IC process.

Considering especially the twisting motion predicted by the CASSCF calculations, one could expect an influence of the solvents viscosity on the TA traces. Thus, additional TA experiments were conducted in the highly viscous ethylene glycol. A direct comparison between selected TA traces in all employed solvents is shown in Figure SI8. A higher amount of excited state absorption was observed for TA traces of *o*-NP in ethylene glycol, leading to superposition of excited state absorption and stimulated emission even for probe wavelengths in the NIR. As a consequence, an unambiguous influence of viscosity on the time constant $\tau_{ind,solv}$ for the stimulated emission decay and, thus, for the structural changes in S_1 is not possible.

In comparison to the transient absorption, faster time constants are obtained in the gas phase as the rotation is not hindered by the surrounding liquid. Moreover, because the time resolution of our liquid phase experiments does not allow us to see $a \leq 20$ fs shift, we observe apparently instantaneous stimulated emission up to the NIR region. The proposed relaxation pathway is sketched in Figure 7. The transiently formed *aci*-nitro isomer of *o*-NP is observed both in the gas and in the liquid phase.

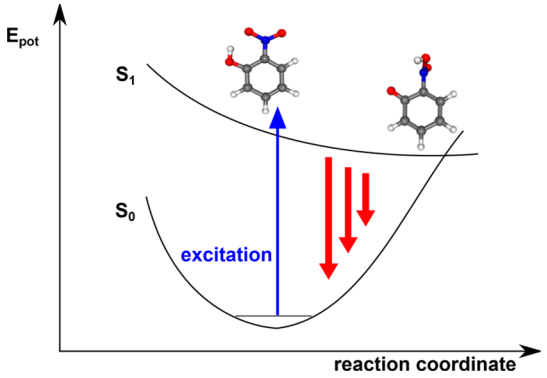

Figure 7. IC part of the proposed relaxation pathway of *o*-NP on the subpicosecond time scale via conical intersection upon excitation into S_1. Relaxation along the reaction coordinate (ESIPT coupled with out-of-plane rotation of the newly formed HONO group) leads to a close approach of S_1 and S_0. In the gas phase, a shift of the onset of the photoelectron spectrum indicates formation of the *aci*-nitro form of *o*-NP (right-hand side structure), whereas stimulated emission (indicated by red arrows) is observed in solution. For more details, see text.

Formation of an intermediate species triggered by ESIPT has also been observed for *o*-nitrobenzaldehyde,[59] finally resulting in an ultrafast fluorescence decay <100 fs. Nevertheless, one would expect an influence on corresponding time constants for the ESIPT reaction caused by different polarities and/or capabilities of hydrogen bonding of the solvent.[60,61] For *o*-NP, however, no significant influence on $\tau_{ind,solv}$ is found, indicating a barrierless reaction coordinate toward CI with the ground state as known from literature.[62] This finding is in line with our CASSCF calculations, as already discussed before. Furthermore, in this study, ESIPT is additionally influenced by a twist of the

DOI: 10.1021/acs.jpca.5b04900
J. Phys. Chem. A XXXX, XXX, XXX−XXX

formed HONO group and, thus, by a twist of the acceptor group. The latter effect can lead to ultrafast IC with S_0 as also observed in earlier studies.[63,64]

4.2. Relaxation via Intersystem Crossing. Considering the stable photoelectron band structure (Figure 3) as well as the remaining transient absorption in *n*-hexane (480 nm, Figure SI5a) and 2-propanol (480 and 500 nm, Figure SI5b,c), formation of a long-lived excited species is observed both in the gas and in the liquid phase. In the liquid phase, the wavelength of the residual absorption is in good agreement with a possible transition originating from T_1 at about 2.57 eV (~482 nm; Table 2 in section 3.4). The transitions with higher or lower excitation energies, which also have non-negligible oscillator strengths, could not be detected because they lie outside the range of our probe wavelengths. Thus, the lifetime of the first excited triplet state T_1 can be attributed to the time constant $\tau_{3,solv}$ (>100 ps in 2-propanol and >500 ps in *n*-hexane) and $\tau_{2,gas}$ (outside of the accessible time window of 700 ps). These assignments are in line with results of a previous study by Takezaki et al.,[13] who determined the lifetime of the first excited triplet state of *o*-NP in benzene to be 900 ± 50 ps. The values determined in our study can be rationalized by consideration of efficiently energy coupling of excited molecules to the surrounding solvent. Thus, it is reasonable that the shortest value of $\tau_{3,solv}$ was found for 2-propanol due to its polarity. Furthermore, this partial relaxation into T_1 is supported by the theoretical study on HONO formation on the triplet PES by Cheng et al.[19]

Concerning the $\pi\pi^*$ character of the first excited singlet state, it is well-known that such states can undergo ISC processes into $^3(n\pi^*)$ states given a small energy gap between those states, as predicted by the El-Sayed selection rules.[65,66] As shown in Figure 2, close-lying triplet states are computed by TD-DFT. Moreover, the evolution of the triplet states along the hydrogen transfer coordinate was calculated at the TD-DFT level of theory (Figure SI9), revealing an intersection of the PES of S_1 (A′) and T_2 (A″) at a (O)H---O(NO) distance of 1.45 Å.

Consequently, the obtained time constant $\tau_{1,solv} \sim 0.4-0.5$ ps as well as $\tau_{1,gas} = 130 \pm 10$ fs can be partly assigned to depopulation of S_1 via ISC. As can be realized from Table 1, the values of $\tau_{1,solv}$ for the different solvents are very close to each other. Because depopulation of S_1 via the aforementioned IC process is a competitive relaxation channel $\tau_{1,solv}$ and $\tau_{1,gas}$ have to be regarded as a lower limit to the ISC process. When gas and liquid phase experiments are compared, smaller time constants are observed in the gas phase as the solvent environment may change the energy levels of the close lying S_1 and triplet states such that ISC is decelerated. An alternative explanation is the acceleration of IC dynamics in the gas phase caused by missing interactions with solvent molecules. Compared to the literature values, the obtained values of $\tau_{1,solv}$ in our study confirm the upper limit estimated by Takezaki et al. in benzene (≤50 ps).[13] Subpicosecond time constants for ISC have been observed for a large number of nitrated polycyclic aromatic compounds.[67−69] In such systems, fast ISC was considered to be the key radiationless process facilitated by a very low energy gap between the first excited singlet and an upper triplet state analogously to the findings for *o*-NP in the present study.

Following these considerations, the additional derived time constant $\tau_{2,solv}$ in solution is then attributable to IC into the lowest lying triplet state, T_1, and vibrational relaxation therein. In analogy to $\tau_{1,solv}$, $\tau_{2,solv}$ is nearly independent of the solvent with an exception being for water, where the value is lower by a factor of 2 as compared to values for the other solvents. In this case energy transfer is most likely facilitated by the higher polarity and proticity of water (dipole moment 1.85 D)[70] compared to the cases of other solvents (*n*-hexane 0 D, chloroform 1.01 D, 2-propanol 1.66 D).[70] For completeness, we note that this channel could also have contributions from hot ground state absorption as a consequence of competitive relaxation processes. Considering the TD-DFT calculations (section 3.4), ISC from S_1 to T_1 is linked to a hydrogen transfer from the hydroxyl to the adjacent nitro group (Figure SI6b). Finally, due to the ultrafast return into the ground state via CI, HONO dissociation is supposed to occur on the triplet manifold. This interpretation is in agreement with assumptions from previous studies.[1,19] In addition, α-ketocarbenes, such as formed during the HONO split-off, may have triplet ground states as demonstrated in several studies.[71−73] The reactivity of various α-ketocarbenes has been found to be governed by the triplet multiplicity of these systems.[71] The proposed relaxation pathway of *o*-NP via ISC is sketched in Figure 8.

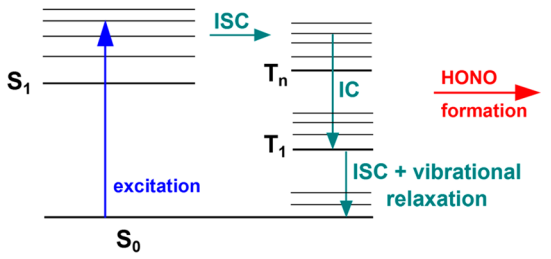

Figure 8. ISC part of the proposed relaxation pathway of *o*-NP. Depopulation of S_1 via ultrafast ISC into upper triplet states was found in solution as well as in the gas phase. HONO release is supposed to take place on the triplet manifold. For more details, see text.

5. CONCLUSION

This study provides the first time-resolved analysis of the photoinduced structural changes in *o*-NP both in the liquid and in the gas phase. The mechanism is governed by the ICT character of the S_1 state. Evidence for the transiently generated *aci*-nitro isomer is obtained, a fact that forms a cornerstone for HONO production in tropospheric *o*-NP photolysis. Due to the observed ultrafast singlet dynamics, the much discussed HONO split-off[1,19] is supposed to take place in the triplet manifold of *o*-NP. A comparison of time-resolved experiments along with results from quantum chemical calculations suggests that the relaxation dynamics of *o*-NP after charge transfer excitation into S_1 ($\pi\pi^*$) are mainly characterized by

(1) Relaxation $S_1 \rightarrow S_0$ via a conical intersection on a subpicosecond time scale characterized by ESIPT in combination with out-of-plane torsion of the newly formed HONO group.
(2) Ultrafast ISC into a triplet manifold on a similar time scale as a competitive relaxation process facilitated by the nearly isoenergetic character of triplet states below S_1, in accordance with the El-Sayed selection rules.[65,66]
(3) HONO formation from within the triplet manifold in competition to vibrational relaxation and ISC to S_0.

Care is needed, however, in transferring these results to other, apparently similar photochemical systems. From this

DOI: 10.1021/acs.jpca.5b04900
J. Phys. Chem. A XXXX, XXX, XXX−XXX

study of *o*-NP in the gas phase and in different solvents as well as from additional preliminary experiments with other nitrophenols, we conclude that in each case individual interactions between specific molecules and the environment have to be considered.

■ ASSOCIATED CONTENT

Supporting Information

The Supporting Information is available free of charge on the ACS Publications website at DOI: 10.1021/acs.jpca.5b04900.

Excitation energies of singlet and triplet states of *o*-NP, extinction coefficients of *o*-NP at 350 nm, relative amplitudes, Cartesian coordinates of the optimized MECI geometry, TRPES spectrum of *o*-NP excited at 315 nm, analysis of TRPES spectra with excitation at 350 and 315 nm, transient absorption profiles of *o*-NP in chloroform and 2-propanol at 350 nm, transient absorption profiles of *o*-NP in *n*-hexane and 2-propanol at long delay times, geometry optimized structures of S_0 and T_1 of *o*-NP, reference experiments (PDF)

■ AUTHOR INFORMATION

Corresponding Author

*A.-N. Unterreiner. E-mail: andreas.unterreiner@kit.edu. Fax: +49 721 608 46524. Tel: +49 721 608 47807.

Notes

The authors declare no competing financial interest.

■ ACKNOWLEDGMENTS

M. Olzmann and A.-N. Unterreiner acknowledge financial support from the Deutsche Forschungsgemeinschaft (contracts Ol 85/3-1 and UN 108/4-2, respectively). H. A. Ernst is supported by the Karlsruhe School of Optics and Photonics (KSOP). A. Stolow thanks NSERC Canada for financial support. O. Schalk acknowledges funding from the Humboldt foundation. T. J. A. Wolf thanks the Fonds der Chemischen Industrie for a fellowship.

■ REFERENCES

(1) Bejan, I.; Abd El Aal, Y.; Barnes, I.; Benter, T.; Bohn, B.; Wiesen, P.; Kleffmann, J. The Photolysis of Ortho-Nitrophenols: A New Gas Phase Source of HONO. *Phys. Chem. Chem. Phys.* **2006**, *8*, 2028−2035.

(2) Kleffmann, J. Daytime Sources of Nitrous Acid (HONO) in the Atmospheric Boundary Layer. *ChemPhysChem* **2007**, *8*, 1137−1144.

(3) Cheng, S.-B.; Zhou, C.-H.; Yin, H.-M.; Sun, J.-L.; Han, K.-L. Photolysis of o-Nitrobenzaldehyde in the Gas Phase: A New OH* Formation Channel. *ChemPhysChem* **2009**, *10*, 1135−1142.

(4) Chen, J.; Wenger, J. C.; Venables, D. S. Near-Ultraviolet Absorption Cross Sections of Nitrophenols and Their Potential Influence on Tropospheric Oxidation Capacity. *J. Phys. Chem. A* **2011**, *115*, 12235−12242.

(5) Gompper, R.; Wagner, H. U. Donor-Acceptor-Substituted Cyclic π-Electron Systems: Touchstone for Theories and Building Blocks of New Materials. *Angew. Chem.* **1988**, *100*, 1492−1511.

(6) Thomsen, C. L.; Thogersen, J.; Keiding, S. R. Ultrafast Charge-Transfer Dynamics: Studies of p-Nitroaniline in Water and Dioxane. *J. Phys. Chem. A* **1998**, *102*, 1062−1067.

(7) Coto, P. B.; Serrano-Andres, L.; Gustavsson, T.; Fujiwara, T.; Lim, E. C. Intramolecular Charge Transfer and Dual Fluorescence of 4-(Dimethylamino)Benzonitrile: Ultrafast Branching Followed by a Two-Fold Decay Mechanism. *Phys. Chem. Chem. Phys.* **2011**, *13*, 15182−15188.

(8) Leavell, S.; Curl, R. F., Jr. Microwave Spectrum of 2-Nitrophenol. Structure of the Hydrogen Bond. *J. Mol. Spectrosc.* **1973**, *45*, 428−442.

(9) Borisenko, K. B.; Bock, C. W.; Hargittai, I. Intramolecular Hydrogen Bonding and Molecular Geometry of 2-Nitrophenol from a Joint Gas-Phase Electron Diffraction and Ab Initio Molecular Orbital Investigation. *J. Phys. Chem.* **1994**, *98*, 1442−1448.

(10) Namboodiri, K. P. K.; Viswanathan, S.; Ganesan, R.; Bhasu, V. C. J. The Electronic Structure, Spectra, and Reactivity of Nitrophenols. *J. Comput. Chem.* **1981**, *2*, 392−401.

(11) Wang, Y.-Q.; Wang, H.-G.; Zhang, S.-Q.; Pei, K.-M.; Zheng, X.; Phillips, D. L. Resonance Raman Intensity Analysis of the Excited State Proton Transfer Dynamics of 2-Nitrophenol in the Charge-Transfer Band Absorption. *J. Chem. Phys.* **2006**, *125*, 214506.

(12) Alif, A.; Pilichowski, J. F.; Boule, P. Photochemistry and Environment XIII: Phototransformation of 2-Nitrophenol in Aqueous Solution. *J. Photochem. Photobiol., A* **1991**, *59*, 209−219.

(13) Takezaki, M.; Hirota, N.; Terazima, M. Nonradiative Relaxation Processes and Electronically Excited States of Nitrobenzene Studied by Picosecond Time-Resolved Transient Grating Method. *J. Phys. Chem. A* **1997**, *101*, 3443−3448.

(14) Harrison, M. A. J.; Barra, S.; Borghesi, D.; Vione, D.; Arsene, C.; Olariu, R. I. Nitrated Phenols in the Atmosphere: A Review. *Atmos. Environ.* **2005**, *39*, 231−248.

(15) Perner, D.; Ehhalt, D. H.; Paetz, H. W.; Platt, U.; Roeth, E. P.; Volz, A. Hydroxyl Radicals in the Lower Troposphere. *Geophys. Res. Lett.* **1976**, *3*, 466−468.

(16) Alicke, B.; Platt, U.; Stutz, J. Impact of Nitrous Acid Photolysis on the Total Hydroxyl Radical Budget During the Limitation of Oxidant Production/Pianura Padana Produzione di Ozono Study in Milan. *J. Geophys. Res.* **2002**, *107*, LOP9/1−LOP9/17.

(17) Harrison, R. M.; Peak, J. D.; Collins, G. M. Tropospheric Cycle of Nitrous Acid. *J. Geophys. Res.* **1996**, *101*, 14429−14439.

(18) Atkinson, R. Atmospheric Chemistry of VOCs and NO_x. *Atmos. Environ.* **2000**, *34*, 2063−2101.

(19) Cheng, S.-B.; Zhou, C.-H.; Yin, H.-M.; Sun, J.-L.; Han, K.-L. OH Produced from o-Nitrophenol Photolysis: A Combined Experimental and Theoretical Investigation. *J. Chem. Phys.* **2009**, *130*, 234311.

(20) Nagaya, M.; Kudoh, S.; Nakata, M. Infrared Spectrum and Structure of the Aci-Nitro Form of 2-Nitrophenol in a Low-Temperature Argon Matrix. *Chem. Phys. Lett.* **2006**, *427*, 67−71.

(21) Lochbrunner, S.; Larsen, J. J.; Shaffer, J. P.; Schmitt, M.; Schultz, T.; Underwood, J. G.; Stolow, A. Methods and Applications of Femtosecond Time-Resolved Photoelectron Spectroscopy. *J. Electron Spectrosc. Relat. Phenom.* **2000**, *112*, 183−198.

(22) Yang, J. P.; Kappes, M. M.; Hippler, H.; Unterreiner, A. N. Femtosecond Transient Absorption Spectroscopy of Single-Walled Carbon Nanotubes in Aqueous Surfactant Suspensions: Determination of the Lifetime of the Lowest Excited State. *Phys. Chem. Chem. Phys.* **2005**, *7*, 512−517.

(23) Wolf, T. J. A.; Voll, D.; Barner-Kowollik, C.; Unterreiner, A.-N. Elucidating the Early Steps in Photoinitiated Radical Polymerization via Femtosecond Pump-Probe Experiments and DFT Calculations. *Macromolecules (Washington, DC, U. S.)* **2012**, *45*, 2257−2266.

(24) Kozma, I.; Baum, P.; Lochbrunner, S.; Riedle, E. Widely Tunable Sub-30 Fs Ultraviolet Pulses by Chirped Sum Frequency Mixing. *Opt. Express* **2003**, *11*, 3110−3115.

(25) Riedle, E.; Beutter, M.; Lochbrunner, S.; Piel, J.; Schenkl, S.; Spörlein, S.; Zinth, W. Generation of 10 to 50 Fs Pulses Tunable through All of the Visible and the NIR. *Appl. Phys. B: Lasers Opt.* **2000**, *71*, 457−465.

(26) Ahlrichs, R.; Baer, M.; Haeser, M.; Horn, H.; Koelmel, C. Electronic Structure Calculations on Workstation Computers: The Program System Turbomole. *Chem. Phys. Lett.* **1989**, *162*, 165−169.

(27) Treutler, O.; Ahlrichs, R. Efficient Molecular Numerical Integration Schemes. *J. Chem. Phys.* **1995**, *102*, 346−354.

(28) Eichkorn, K.; Treutler, O.; Oehm, H.; Haeser, M.; Ahlrichs, R. Auxiliary Basis Sets to Approximate Coulomb Potentials. *Chem. Phys. Lett.* **1995**, *240*, 283−290.

DOI: 10.1021/acs.jpca.5b04900
J. Phys. Chem. A XXXX, XXX, XXX−XXX

(29) Eichkorn, K.; Treutler, O.; Oehm, H.; Haeser, M.; Ahlrichs, R. Auxiliary Basis Sets to Approximate Coulomb Potentials. [Erratum to Document Cited in Ca123:93649]. *Chem. Phys. Lett.* **1995**, *242*, 652−660.
(30) Eichkorn, K.; Weigend, F.; Treutler, O.; Ahlrichs, R. Auxiliary Basis Sets for Main Row Atoms and Transition Metals and Their Use to Approximate Coulomb Potentials. *Theor. Chem. Acc.* **1997**, *97*, 119−124.
(31) Schaefer, A.; Horn, H.; Ahlrichs, R. Fully Optimized Contracted Gaussian Basis Sets for Atoms Lithium to Krypton. *J. Chem. Phys.* **1992**, *97*, 2571−2577.
(32) Weigend, F. Accurate Coulomb-Fitting Basis Sets for H to Rn. *Phys. Chem. Chem. Phys.* **2006**, *8*, 1057−1065.
(33) Dirac, P. A. M. Quantum Mechanics of Many-Electron Systems. *Proc. R. Soc. London, Ser. A* **1929**, *123*, 714−733.
(34) Slater, J. C. A Simplification of the Hartree-Fock Method. *Phys. Rev.* **1951**, *81*, 385−390.
(35) Vosko, S. H.; Wilk, L.; Nusair, M. Accurate Spin-Dependent Electron Liquid Correlation Energies for Local Spin Density Calculations: A Critical Analysis. *Can. J. Phys.* **1980**, *58*, 1200−1211.
(36) Becke, A. D. Density-Functional Exchange-Energy Approximation with Correct Asymptotic Behavior. *Phys. Rev. A: At., Mol., Opt. Phys.* **1988**, *38*, 3098−3100.
(37) Kendall, R. A.; Dunning, T. H., Jr.; Harrison, R. J. Electron Affinities of the First-Row Atoms Revisited. Systematic Basis Sets and Wave Functions. *J. Chem. Phys.* **1992**, *96*, 6796−6806.
(38) Lee, C.; Yang, W.; Parr, R. G. Development of the Colle-Salvetti Correlation-Energy Formula into a Functional of the Electron Density. *Phys. Rev. B: Condens. Matter Mater. Phys.* **1988**, *37*, 785−789.
(39) Becke, A. D. Density-Functional Thermochemistry. III. The Role of Exact Exchange. *J. Chem. Phys.* **1993**, *98*, 5648−5652.
(40) Bauernschmitt, R.; Ahlrichs, R. Treatment of Electronic Excitations within the Adiabatic Approximation of Time Dependent Density Functional Theory. *Chem. Phys. Lett.* **1996**, *256*, 454−464.
(41) Grimme, S.; Furche, F.; Ahlrichs, R. An Improved Method for Density Functional Calculations of the Frequency-Dependent Optical Rotation. *Chem. Phys. Lett.* **2002**, *361*, 321−328.
(42) Bauernschmitt, R.; Haeser, M.; Treutler, O.; Ahlrichs, R. Calculation of Excitation Energies within Time-Dependent Density Functional Theory Using Auxiliary Basis Set Expansions. *Chem. Phys. Lett.* **1997**, *264*, 573−578.
(43) Schmidt, M. W.; Baldridge, K. K.; Boatz, J. A.; Elbert, S. T.; Gordon, M. S.; Jensen, J. H.; Koseki, S.; Matsunaga, N.; Nguyen, K. A.; Shujun, S.; et al. General Atomic and Molecular Electronic Structure System. *J. Comput. Chem.* **1993**, *14*, 1347−1363.
(44) Gordon, M. S.; Schmidt, M. W. Advances in Electronic Structure Theory: Gamess a Decade Later. In *Theory and Applications of Computational Chemistry: The First Forty Years*; Dykstra, C. E., Frenking, G., Kim, K. S., Scuseria, G. E. Eds.; Elsevier B.V.: Amsterdam, Netherlands, 2005; pp 1167−1189.
(45) Nakano, H. Quasidegenerate Perturbation Theory with Multiconfigurational Self-Consistent-Field Reference Functions. *J. Chem. Phys.* **1993**, *99*, 7983−7992.
(46) Nakano, H. MCSCF Reference Quasidegenerate Perturbation Theory with Epstein-Nesbet Partitioning. *Chem. Phys. Lett.* **1993**, *207*, 372−378.
(47) Kobayashi, T.; Nagakura, S. Photoelectron Spectra of Nitrophenols and Nitroanisoles. *J. Electron Spectrosc. Relat. Phenom.* **1975**, *6*, 421−427.
(48) Wolf, T. J. A.; Kuhlman, T. S.; Schalk, O.; Martinez, T. J.; Møller, K. B.; Stolow, A.; Unterreiner, A. N. Hexamethylcyclopentadiene: Time-Resolved Photoelectron Spectroscopy and Ab Initio Multiple Spawning Simulations. *Phys. Chem. Chem. Phys.* **2014**, *16*, 11770−11779.
(49) Schalk, O.; Boguslavskiy, A. E.; Stolow, A.; Schuurman, M. S. Through-Bond Interactions and the Localization of Excited-State Dynamics. *J. Am. Chem. Soc.* **2011**, *133*, 16451−16458.
(50) Schalk, O.; Schuurman, M. S.; Wu, G.; Lang, P.; Mucke, M.; Feifel, R.; Stolow, A. Internal Conversion versus Intersystem Crossing: What Drives the Gas Phase Dynamics of Cyclic α,β-Enones? *J. Phys. Chem. A* **2014**, *118*, 2279−2287.
(51) Pedersen, S.; Zewail, A. H. Femtosecond Real-Time Probing of Reactions XXII. Kinetic Description of Probe Absorption, Fluorescence, Depletion and Mass Spectrometry. *Mol. Phys.* **1996**, *89*, 1455−1502.
(52) Brackmann, U. *LambdachromeLaser®Dyes*; Lambda Physik GmbH: Göttingen, Germany, 2000.
(53) Schriever, C.; Lochbrunner, S.; Ofial, A. R.; Riedle, E. The Origin of Ultrafast Proton Transfer: Multidimensional Wave Packet Motion vs. Tunneling. *Chem. Phys. Lett.* **2011**, *503*, 61−65.
(54) Lochbrunner, S.; Schultz, T.; Schmitt, M.; Shaffer, J. P.; Zgierski, M. Z.; Stolow, A. Dynamics of Excited-State Proton Transfer Systems via Time-Resolved Photoelectron Spectroscopy. *J. Chem. Phys.* **2001**, *114*, 2519−2522.
(55) Grabowski, Z. R.; Rotkiewicz, K.; Rettig, W. Structural Changes Accompanying Intramolecular Electron Transfer: Focus on Twisted Intramolecular Charge-Transfer States and Structures. *Chem. Rev. (Washington, DC, U. S.)* **2003**, *103*, 3899−4031.
(56) Grabowski, Z. R.; Rotkiewicz, K.; Siemiarczuk, A. Dual Fluorescence of Donor-Acceptor Molecules and the Twisted Intramolecular Charge Transfer (TICT) States. *J. Lumin.* **1979**, *18*−*19*, 420−424.
(57) Barbatti, M.; Aquino, A. J. A.; Lischka, H.; Schriever, C.; Lochbrunner, S.; Riedle, E. Ultrafast Internal Conversion Pathway and Mechanism in 2-(2′-Hydroxyphenyl)Benzothiazole: A Case Study for Excited-State Intramolecular Proton Transfer Systems. *Phys. Chem. Chem. Phys.* **2009**, *11*, 1406−1415.
(58) Polli, D.; Altoe, P.; Weingart, O.; Spillane, K. M.; Manzoni, C.; Brida, D.; Tomasello, G.; Orlandi, G.; Kukura, P.; Mathies, R. A.; et al. Conical Intersection Dynamics of the Primary Photoisomerization Event in Vision. *Nature (London, U. K.)* **2010**, *467*, 440−443.
(59) Heinz, B.; Schmierer, T.; Laimgruber, S.; Gilch, P. Excited State Processes of Nitrobenzaldehydes Probed by Ultrafast Fluorescence and Absorption Spectroscopy. *J. Photochem. Photobiol., A* **2008**, *199*, 274−281.
(60) Lochbrunner, S.; Wurzer, A. J.; Riedle, E. Microscopic Mechanism of Ultrafast Excited-State Intramolecular Proton Transfer: A 30-Fs Study of 2-(2′-Hydroxyphenyl)Benzothiazole. *J. Phys. Chem. A* **2003**, *107*, 10580−10590.
(61) Huston, A. L.; Scott, G. W.; Gupta, A. Mechanism and Kinetics of Excited-State Relaxation in Internally Hydrogen-Bonded Molecules: 2-(2′-Hydroxy-5′-Methylphenyl)-Benzotriazole in Solution. *J. Chem. Phys.* **1982**, *76*, 4978−4985.
(62) Hu, S.; Liu, K.; Li, Y.; Ding, Q.; Peng, W.; Chen, M. Investigation of Excited-State Intramolecular Proton Transfer Coupled Charge Transfer Reaction of Paeonol. *Can. J. Chem.* **2014**, *92*, 274−278.
(63) Farztdinov, V. M.; Schanz, R.; Kovalenko, S. A.; Ernsting, N. P. Relaxation of Optically Excited p-Nitroaniline: Semiempirical Quantum-Chemical Calculations Compared to Femtosecond Experimental Results. *J. Phys. Chem. A* **2000**, *104*, 11486−11496.
(64) Kovalenko, S. A.; Schanz, R.; Farztdinov, V. M.; Hennig, H.; Ernsting, N. P. Femtosecond Relaxation of Photoexcited Para-Nitroaniline: Solvation, Charge Transfer, Internal Conversion and Cooling. *Chem. Phys. Lett.* **2000**, *323*, 312−322.
(65) El-Sayed, M. A. Spin-Orbit Coupling and the Radiationless Processes in Nitrogen Heterocyclics. *J. Chem. Phys.* **1963**, *38*, 2834−2838.
(66) Lower, S. K.; El-Sayed, M. A. Triplet State and Molecular Electronic Processes in Organic Molecules. *Chem. Rev.* **1966**, *66*, 199−241.
(67) Zugazagoitia, J. S.; Almora-Diaz, C. X.; Peon, J. Ultrafast Intersystem Crossing in 1-Nitronaphthalene. An Experimental and Computational Study. *J. Phys. Chem. A* **2008**, *112*, 358−365.
(68) Collado-Fregoso, E.; Zugazagoitia, J. S.; Plaza-Medina, E. F.; Peon, J. Excited-State Dynamics of Nitrated Push-Pull Molecules: The Importance of the Relative Energy of the Singlet and Triplet Manifolds. *J. Phys. Chem. A* **2009**, *113*, 13498−13508.

DOI: 10.1021/acs.jpca.5b04900
J. Phys. Chem. A XXXX, XXX, XXX−XXX

(69) Plaza-Medina, E. F.; Rodriguez-Cordoba, W.; Peon, J. Role of Upper Triplet States on the Photophysics of Nitrated Polyaromatic Compounds: S_1 Lifetimes of Singly Nitrated Pyrenes. *J. Phys. Chem. A* **2011**, *115*, 9782−9789.
(70) Haynes, W. M. *Handbook of Chemistry and Physics*; CRC Press: London, U.K., 2011.
(71) Bonnichon, F.; Richard, C.; Grabner, G. Formation of an α-Ketocarbene by Photolysis of Aqueous 2-Bromophenol. *Chem. Commun. (Cambridge, U. K.)* **2001**, 73−74.
(72) Grabner, G.; Richard, C.; Koehler, G. Formation and Reactivity of 4-Oxocyclohexa-2,5-Dienylidene in the Photolysis of 4-Chlorophenol in Aqueous Solution at Ambient Temperature. *J. Am. Chem. Soc.* **1994**, *116*, 11470−11480.
(73) McMahon, R. J.; Chapman, O. L.; Hayes, R. A.; Hess, T. C.; Krimmer, H. P. Mechanistic Studies on the Wolff Rearrangement: The Chemistry and Spectroscopy of Some α-Keto Carbenes. *J. Am. Chem. Soc.* **1985**, *107*, 7597−7606.

DOI: 10.1021/acs.jpca.5b04900
J. Phys. Chem. A XXXX, XXX, XXX−XXX